Low-temperature anisotropic diffusion of helium in zircon: Implications for zircon (U–Th)/He thermochronometry

Martin Reich [a,b,*], Rodney C. Ewing [a], Todd A. Ehlers [a], Udo Becker [a]

[a] *Department of Geological Sciences, University of Michigan, Ann Arbor, MI 48109-1063, USA*
[b] *Departamento de Geología, Facultad de Ciencias Físicas y Matemáticas, Universidad de Chile, Santiago, Chile*

Abstract

In the last decade the zircon (U–Th)/He (ZHe) thermochronometer has been applied to a variety of geologic problems. Although bulk diffusion coefficients for He in zircon are available from laboratory step-heating experiments, little is known about the diffusion mechanism(s) and their dependence on the crystallographic structure of zircon. Here, we investigate the diffusion of He in perfectly crystalline zircon using atomistic simulation methods that provide insights into the structural pathways of He migration in zircon. Empirical force fields and quantum-mechanical calculations reveal that the energy barriers for He diffusion are strongly dependent on structure. The most favorable pathway for He diffusion is the [0 0 1] direction through the open channels parallel to the *c*-axis ($\Delta E^*_{[001]} = 13.4$ kJ mol^{-1}, activation energy for tracer diffusion of a He atom along [0 0 1]). In contrast, energy barriers are higher in other directions where narrower channels for He diffusion are identified, such as [1 0 0], [1 0 1], and [1 1 0] (ΔE^* of 44.8, 101.7, and 421.3 kJ mol^{-1}, respectively). Molecular dynamics simulations are in agreement with these results and provide additional insight in the diffusion mechanisms along different crystallographic directions, as well as the temperature dependence. Below the closure temperature of He in zircon [$T_c \sim 180$ °C, Reiners P. W., Spell T. L., Nicolescu S., and Zanetti K. A. (2004) Zircon (U–Th)/He thermochronometry: He diffusion and comparisons with Ar-40/Ar-39 dating. *Geochim. Cosmochim. Acta* **68**, 1857–1887], diffusion is anisotropic as He moves preferentially along the [0 0 1] direction, and calculated tracer diffusivities along the two most favorable directions differ by approximately five orders of magnitude ($D_{[001]}/D_{[100]} \sim 10^5$, at $T = 25$ °C). Above this temperature, He atoms start to hop between adjacent [0 0 1] channels, along [1 0 0] and [0 1 0] directions (perpendicular to the *c*-axis). The diffusion along [1 0 0] and [0 1 0] is thermally activated, such that at higher temperatures, He diffusion in zircon becomes nearly isotropic ($D_{[001]}/D_{[100]} \sim 10$, at $T = 580$ °C). These results suggest that the anisotropic nature of He diffusion at temperatures near the closure temperature should be considered in future diffusivity experiments. Furthermore, care should be taken when making geologic interpretations (e.g., exhumation rates, timing of cooling, etc.) from this thermochronometer until the effects of anisotropic diffusion on bulk ages and closure temperature estimates are better quantified.

1. INTRODUCTION

Zircon ($ZrSiO_4$) occurs ubiquitously in a wide range of geological environments and rock types where it can accommodate minor to trace amounts of actinides and lanthanides (Finch and Hanchar, 2003). Its refractory nature throughout geologic cycles has made zircon an essential mineral in investigations of the geochemical and isotopic evolution of the crust, even at ages close to the Earth's formation (Valley et al., 2002; Watson and Harrison, 2005). The fact that zircon incorporates U and Th in high-temperature processes, such as igneous crystallization or metamorphism (>750 °C), coupled to its resistance to physical abrasion and chemical weathering, have made zircon the

* Corresponding author. Address: Departamento de Geología, Facultad de Ciencias Físicas y Matemáticas, Universidad de Chile, Santiago, Chile. Fax: +56 2 6963050.
E-mail addresses: mreichm@umich.edu, mreich@cec.uchile.cl (M. Reich).

primary mineral used in U/Pb geochronology. In addition, the same decay chains that produce radiogenic Pb from U and Th in zircon also produce radiogenic He. More recently, zircon (U–Th)/He (ZHe) decay has been proposed as a low-temperature thermochronometer with a closure temperature of ~180–200 °C (Farley, 2002; Reiners et al., 2002, 2004; Tagami et al., 2003; Reiners, 2005).

However, the main complication that arises in ZHe chronology relates to the characteristics of He diffusion. Extensive radiation damage and slow damage annealing rates (Weber et al., 1994; Meldrum et al., 1998; Ewing et al., 2003; Palenik et al., 2003) can potentially have a significant effect on He diffusion (Farley et al., 1996; Farley, 2000; Shuster et al., 2006), although Reiners et al. (2004) showed that these effects are not significant for dosages up to $2–4 \times 10^{18}$ α-decay events per gram. Unlike elements such as Pb, O, and the rare earth elements (Watson and Cherniak, 1997; Cherniak et al., 1997a,b; Cherniak and Watson, 2001, 2003), experimental diffusivity data for He in zircon are limited, and the mechanism(s) that control the diffusion of He are still not well understood. He diffusion experiments by Reiners et al. (2004) on zircons of varying ages and U–Th contents yield an average activation energy $E_a = 40.4 \pm 0.9$ kcal mol^{-1} (169 ± 3.8 kJ mol^{-1}) and an average pre-exponential factor $D_0 = 0.46^{+0.87}_{-0.30}$ cm^2 s^{-1}. Based on these data and specific assumptions on grain sizes and cooling rates, closure temperatures (T_c, Dodson, 1973) for He diffusion in zircon are calculated to be between ~170–200 °C (Reiners et al., 2004). Although these data constrain the bulk diffusivity of He in zircon as a function of temperature, no information is available on the anisotropy of the diffusivity. Furthermore, previously derived bulk diffusivities and closure temperatures do not provide information on the atomic-scale interactions between He and Zr, Si, and O in zircon. This information is essential to defining the most favorable mechanisms and structural pathways for He diffusion within zircon. In addition, these data are necessary to better evaluate the origin of non-Arrhenius behavior previously documented in early stages of He diffusion experiments (Fig. 1), such as, e.g., structurally-controlled anisotropic diffusion, inhomogeneous distribution of He, and/or localized high-diffusivity from small high-radiation damage zones (Reiners et al., 2002, 2004; Reiners, 2005).

In this study, we use different computer simulations in order to elucidate the atomistic details of He diffusion in perfectly crystalline zircon. Using empirical force fields and quantum-mechanical methods, we determined the most energetically favorable pathways for He diffusion in zircon, by calculating their respective energy barriers as a function of crystallographic direction. These results are further investigated by molecular dynamics simulations in order to gain insight into the mechanisms of He diffusion in zircon as a function of temperature.

2. METHODS

In general, atomistic simulation methods are based on the concept that the total energy of a crystal structure can be obtained by calculating the interactions between their constituent atoms (Dove, 2001). Thus, the energy barriers (activation energies) and He diffusivities can be calculated as a function of crystallographic direction and temperature by calculating the most energetically favorable pathways for He diffusion in the zircon structure. In addition, the atomistic mechanism(s) of He diffusion in the zircon structure can be constrained using dynamic methods, providing valuable information that cannot be extracted from bulk-scale laboratory diffusivity experiments. Examples on the application of these methods in materials science and physical-chemistry can be found on Maca et al. (1999) and Van den Berg et al. (2005).

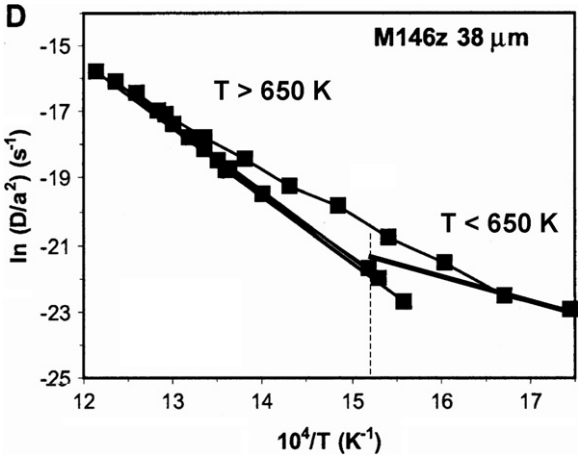

Fig. 1. Arrhenius plot of a cycled step-heating He diffusion experiment on a 66 μm zircon, modified from Reiners et al. (2004). Non-Arrhenius behavior is observed at $T < 650$ K, suggesting a change in the mechanism of He diffusion in zircon. Solid lines represent the two different slopes.

2.1. Interatomic potentials

The first step in quantifying the diffusion of He in zircon is to construct an interatomic potential set that predicts the crystal structure and physical properties of zircon, and that at the same time describes the atomic interactions between He and Zr, Si, and O in zircon. In this study, the interatomic potentials were obtained by combining empirical force fields and the quantum-mechanical approach.

2.1.1. Empirical force field for zircon

The interatomic potentials (U_{GULP}) for Zr–O, Si–O, and O–O interactions in zircon can be defined as a sum of long-range (Coulomb) and short-range (Born-Mayer) potentials, as it is expressed in Eq. (1):

$$U_{GULP} = \sum_{i,j} \left(-\frac{|q_i q_j|}{4\pi\varepsilon_0 r_{ij}} + A_{ij} \exp\left[\frac{-r_{ij}}{\rho_0}\right] \right) \quad (1)$$

The first term on the right-hand side of Eq. (1) stands for the Coulomb interaction, where q_i and q_j are the charges of the atoms, ε_0 is the permittivity of free space, and r_{ij} is the distance between the two atoms. The Born-Mayer-type term (second term on the right-hand side of Eq. (1)) represents the non-bonded, short-range repulsive interactions

where A_{ij} and ρ_0 are empirical constants depending on the atom pair. The parameters of the Born-Mayer potential for Zr–O, Si–O, and O–O interactions were taken from Devanathan et al. (2004) (Table 1). Geometry optimization of the zircon structure was performed using the General Utility Lattice Program GULP (Gale and Rohl, 2003), and good agreement was found between experimental and calculated structure and physical properties for zircon (Table 2).

2.1.2. Quantum-mechanical interactions for He

The interatomic potentials between He and Zr, Si, and O in zircon were determined using a quantum-mechanical approach. This method was chosen to model the interaction between neutral He and the charged species in zircon. These interactions cannot be captured using empirical force fields methods, due to the lack of Coulomb contribution for He interactions resulting from the neutral charge of He.

The quantum-mechanical code GAUSSIAN 03 (Frisch et al., 2004) was used to calculate the energy of the He–Zr, He–Si, and He–O pair interactions, as a function of interatomic distance. Numerical solutions to the Schrödinger equation $\boldsymbol{H}\Psi = E\Psi$ were obtained by using Gaussian-type wavefunctions (6-31g*) as trial functions along with a hybrid Hartree–Fock/DFT theory level (B3LYP functional; Becke, 1993). The potential energy (U_{GAUSS}) vs. distance (r) data for each atomic pair (calculated using GAUSSIAN), were then fitted to Born-Mayer potentials of the type $U_{GAUSS} = A_{ij}\exp(r_{ij}/\rho_0)$. This allow us to extract the A_{ij} and ρ_0 parameters (Table 1), as shown in Fig. 2 for the He–O case (for O, Zr, and Si, their formal charge was applied in these cluster calculations).

Table 1
Born-Mayer pair-potential parameters used for geometry optimization of zircon (taken from Devanathan et al., 2004)

Pair interaction	A_{ij} (kJ mol^{-1})	ρ_0 (Å)	Charges
Zr–O	5225.31	0.305004	Zr: + 3.8
Si–O	3389.91	0.227225	Si: + 2.0
O–O	4662.15	0.306820	O: −1.45
He–Zr	154515.12	0.240800	Zr: + 4.0
He–Si	164975.12	0.189100	Si: + 4.0
He–O	31622.67	0.302700	O: −2.0

Helium interactions calculated from first-principles using GAUSSIAN.

2.2. Energy barrier calculations

2.2.1. Structural pathways in zircon

Energy barrier calculations were conducted to determine preferential pathways for He diffusion in zircon, as a function of crystallographic direction. Preferential diffusion paths were determined by geometric examination of the zircon structure (Fig. 3a–d). The principal structural unit of zircon ($I4_1/amd$) is defined by a chain of alternating edge-sharing [SiO_4] tetrahedra and [ZrO_8] triangular dodecahedra parallel to [0 0 1] direction (c-axis) (Robinson et al., 1971). These chains are laterally ($\perp$ [0 0 1]) joined by edge-sharing dodecahedra, leaving open channels or

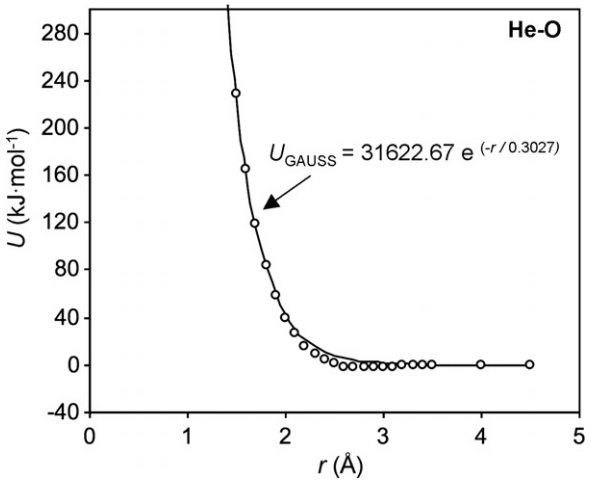

Fig. 2. He–O pair interaction calculated from quantum-mechanics using GAUSSIAN (open circles). Data was fitted to a Born-Mayer potential (solid line).

Table 2
Calculated versus experimental structure parameters and physical properties for zircon after geometry optimization using GULP

Parameter	Units	Experimental value[a]	Calculated value	Difference	% Difference
a	Å	6.607	6.602	−0.005	−0.08
b	Å	6.607	6.602	−0.005	−0.08
c	Å	5.982	6.093	0.111	1.86
Volume	Å^3	261.129	265.593	4.463931	1.71

Elastic constants tensor (units = 10^{11} Dyne cm^{-2} = 10 GPa)

Indices	1	2	3	4	5	6	Experimental[b]
1	44.54	6.41	13.32	0.00	0.00	0.00	$C_{11} = 42.37$
2	6.41	44.54	13.32	0.00	0.00	0.00	$C_{12} = 7.03$
3	13.32	13.32	47.92	0.00	0.00	0.00	$C_{13} = 14.95$
4	0.00	0.00	0.00	8.44	0.00	0.00	$C_{33} = 49.00$
5	0.00	0.00	0.00	0.00	8.44	0.00	$C_{44} = 11.36$
6	0.00	0.00	0.00	0.00	0.00	6.39	

[a] Robinson et al. (1971).
[b] Ozkan et al. (1974).

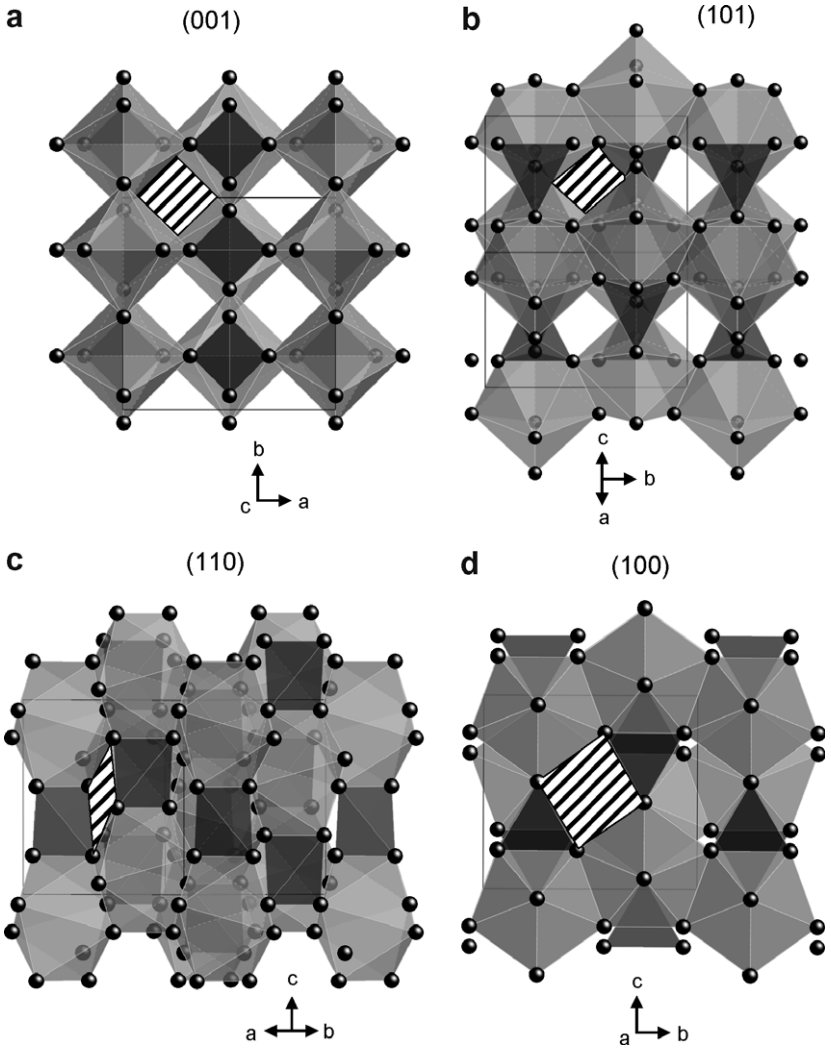

Fig. 3. Polyhedral models of the zircon structure along different crystallographic orientations. Channels for He diffusion are identified along [001], [101], [110], and [100] directions (striped areas). Black spheres are oxygen atoms, and grey and black polyhedra contain a zirconium and silica atom in the center, respectively. Miller indices in parenthesis indicate a crystal face, while numbers in brackets indicate its zone axis ($\perp$ crystal face). Zircon models were constructed using Crystal Maker 6.0.

"pipes" that can allow the diffusion of He along the [001] direction (Fig. 3a). Other potential channels for He diffusion occur along the [101] and [110] directions (Fig. 3b and c, respectively), although these are considerably narrower than the [001] channels. Finally, the [100] and the symmetry-equivalent [010] directions have the least continuous paths from a geometric point of view (Fig. 3d), consisting of open cavities that occur along [100] and [010] directions but that are periodically blocked by Zr edge-sharing dodecahedra (Fig. 3d).

2.2.2. Static total-energy calculations

The energetics of He diffusion along the previously defined crystallographic pathways in zircon ([001], [100], [101], and [110]) were calculated using the force field described in Section 2.1. The empirical force field data for zircon and the quantum-mechanically derived He–X interactions (X = Zr, O, Si) were combined into a single force field and transferred to Materials Studio 4.0 software package (Accelrys, 2005). A $3 \times 3 \times 3$ zircon supercell (649 atoms) was constructed, and the lowest energy position for an incorporated single ^{4}He atom was obtained after geometry optimization of the supercell. The lowest energy position for He in the zircon superlattice (8.25, 9.78, and 11.65 Å) is located in the center of a square cavity cut perpendicular to the *c*-axis (Fig. 3a). The He atom can then be visualized as sitting approximately in the geometric center of the zircon superlattice, inside one of the [001] channels.

The energy barrier profiles (DE^* versus distance) for the diffusion of He along the [001], [100], [101], and [110] directions were obtained by calculating the total energy of the zircon supercell for different He positions, i.e., the He atom is sequentially moved between two energy minima in steps of 0.1 Å along a particular direction path, and the total energy is calculated at each incremental step, keeping the He atom coordinates fixed and letting the rest of the structure relax during the geometry optimization. The calculated total energy in electron volts (eV) reflects the energy

barrier for a single He atom to diffuse between two minima in the zircon structure. We also convert these energies to macroscopic units (kJ mol^{-1}) to make our results more easily comparable to bulk experimental data available.

2.3. Molecular dynamics simulations

The atomistic methods previously described provide valuable information about the energetics of He diffusion in zircon along specific structural directions, but do not yield dynamical information about the system. This dynamic picture is necessary to investigate the mechanisms of He diffusion in zircon as a function of time and temperature. Molecular dynamics (MD) simulations can provide information on the temperature dependence and the mechanism(s) involved in the diffusion process. The classical MD computer simulation technique involves solving Newton's equations of motions for a system of interacting particles, in this case atoms, as a function of time and temperature (Garofalini, 2001; and references therein). The major advantage of MD is the ability to evaluate properties over the whole system or over specific structural units of interest within the system of atoms, e.g., offering the possibility of evaluating diffusion paths and mechanisms. Therefore, movies of the atomistic diffusion process at different temperatures can be obtained by analyzing the trajectories of the atoms as a function of time.

The temperature-dependent diffusion of He in zircon was evaluated using MD simulations performed in a $3 \times 3 \times 3$ supercell of perfectly crystalline zircon containing one ^{4}He atom. Periodic boundary conditions were employed in all simulations to model zircon as an infinite three-dimensional crystal with no edge effects. Due to the periodic nature of the system and because we are interested in the temperature dependence of the diffusion process, a constant NPT ensemble (Number of atoms, Pressure, and Temperature, respectively) was applied. The time step in these calculations was 10 fs with an equilibration time of 5 ps (500 time steps) and a production/observation time of 5 ps. Interatomic potentials were taken from Table 1. The simulations were performed at 300, 450, 650, 850, and 1050 K, that is, below and above the average closure temperature (~450 K, ~180 °C) reported by Reiners et al. (2004).

3. RESULTS

3.1. Energy barriers

The results of the energy barrier calculations for the diffusion of He in zircon along different crystallographic directions are presented in Fig. 4 and Table 3. The energy barrier (ΔE^*) is defined as the activation energy for diffusion of a He atom between two energy minima, along a particular direction (see Section 2.2). The results reveal different ΔE^* values along the four potential diffusion channels of the zircon structure ([0 0 1], [1 0 0]/[0 1 0], [1 0 1], and [1 1 0]). The most energetically favorable path for He diffusion in zircon is [0 0 1], with a $\Delta E^*_{[001]}$ of 13.4 kJ mol^{-1} (3.2 kcal mol^{-1}, 0.1 eV) (Fig. 4a, [0 0 1]). The energy profile between two minima (distance of ~2.2 Å) is mostly flat, due to relatively open channels of the zircon structure along [0 0 1].

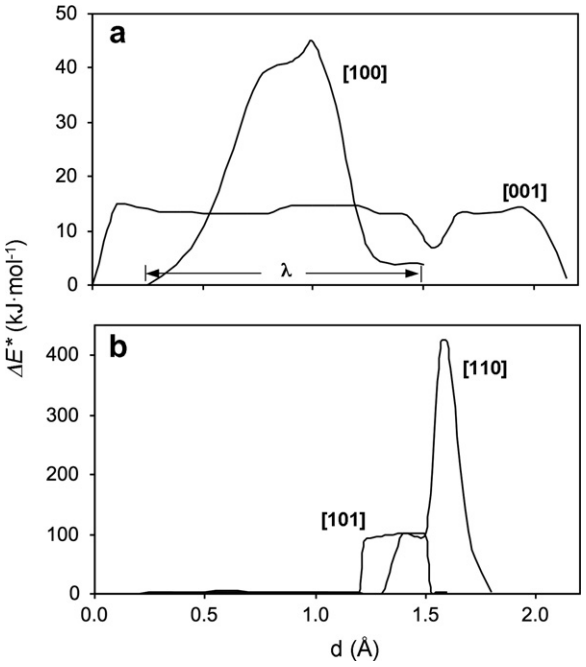

Fig. 4. Energy barriers ΔE^* (or activation energies E_a) versus distance between two minima for He diffusion in zircon along [1 0 0], [0 0 1], [1 0 1], and [1 1 0], as calculated from empirical force fields and quantum-mechanics. The jump distance (λ) for the [1 0 0] direction is depicted.

Table 3
Calculated energy barriers ΔE^* (or activation energies E_a) for He diffusion in zircon along different crystallographic directions

Zone axes	λ (Å)	$\Delta E^*(E_a)$		
		kJ mol^{-1}	kcal mol^{-1}	eV
[0 0 1]	2.20	13.4	3.2	0.1
[1 0 0]	1.25	44.8	10.7	0.5
[1 0 1]	0.30	101.7	24.3	1.1
[1 1 0]	0.50	421.3	100.7	4.4

Lambda (λ) is the jump distance in Å.

Diffusion of He along [1 0 0] (or [0 1 0]) shows an energy barrier ($\Delta E^*_{[100]}$) of 44.8 kJ mol^{-1} (10.7 kcal mol^{-1}, 0.5 eV), approximately 3.5 times higher than $\Delta E^*_{(001)}$ (Fig. 4a, [1 0 0]). As seen in Fig. 4a, the energy profile as a function of distance shows a bell-like shape, with the maximum energy approximately halfway between the two minima (distance between minima ~1.25 Å). Finally, the highest ΔE^* is calculated for the [1 0 1] and [1 1 0] directions, with energy barriers of 101.7 kJ mol^{-1} (24.3 kcal mol^{-1}, 1.1 eV), and 421.3 kJ mol^{-1} (100.7 kcal mol^{-1}, 4.4 eV), respectively (Fig. 4b).

3.2. Mechanisms and temperature dependence

Selected frames of molecular dynamics simulations of He diffusion in a $3 \times 3 \times 3$ supercell are presented in Fig. 5, at three temperatures (300, 450, and 850 K, below,

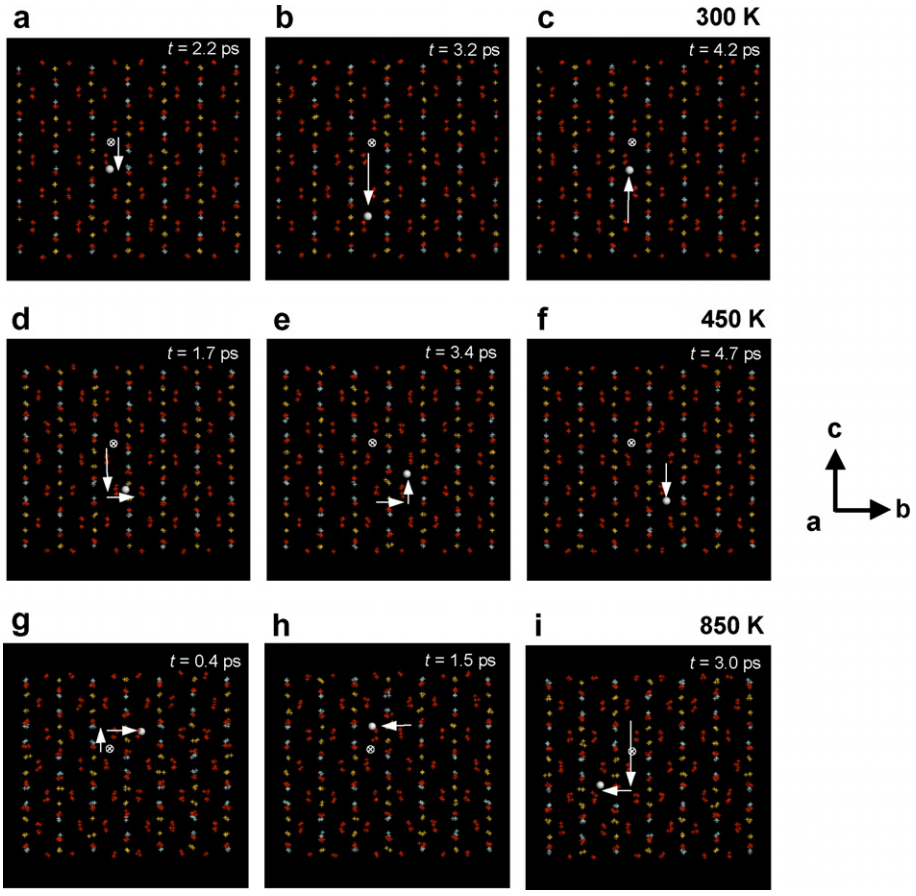

Fig. 5. Selected frames of molecular dynamics (MD) simulations at 300 K (a–c), 340 K (d–f), and 850 K (g–i). The white sphere is the diffusing He atom. The starting position of He, before diffusion, is shown as a white circled cross, and the arrows represent the trajectory of the He atom. Red, cyan, and yellow crosses are oxygen, zirconium, and silicon atoms, respectively. Time step of the simulation (in picoseconds) is depicted on the upper right corner of each frame.

at and above the T_c, respectively). The starting simulation cell for each temperature run is oriented parallel to the *c*-axis, perpendicular to the [0 1 0] direction. As a reference, the vertical rows of atoms define the limits (or "walls") of the open channels or "pipes" parallel to the *c*-axis. Five movies of the MD simulations (300, 450, 650, 850, and 1050 K; 20 s each) can be seen at http://www.geo.lsa.umich.edu/compmin/members/reichch5.htm.

At room temperature (300 K, Fig. 5a–c, Movie 1), He diffuses only along the [0 0 1] direction. No displacement of the He atom was observed along any other direction at this temperature. When the temperature of the simulation is increased to 450 K (~180 °C, T_c of He in zircon), He still diffuses preferentially along the [0 0 1] direction. However, a single horizontal jump of the He atom can be observed at this temperature during the time of simulation, along [1 0 0] (Fig. 5d–f, Movie 2). At a higher temperature (above T_c, 650 K), He diffusion along [1 0 0] occurs more frequently (Movie 3). Finally, at 850 and 1050 K, the frequency of "hopping" between channels ∥ [0 0 1] increases. At these temperatures, He diffuses in both the [0 0 1] and [1 0 0] directions (Fig. 5g–i, Movies 4 and 5).

4. DISCUSSION

4.1. Energetics and mechanisms of He diffusion

The energetics of He diffusion in zircon depends strongly on the crystallographic orientation (Table 3; Figs. 4, 5; Movies 1–5). Based on the magnitude of the diffusion barriers (Table 3), we conclude that diffusion of He ∥ [0 0 1] is the most energetically favorable, with $\Delta E^*_{[001]} = 13.4\ \mathrm{kJ\ mol^{-1}}$, ~5.4 times the thermal energy $k_B T$, at room temperature (k_B = Boltzmann's constant = $1.38 \times 10^{-26}\ \mathrm{kJ\ K^{-1}}$). Therefore, a He atom can move freely along the open channels parallel to the *c*-axis (Fig. 3a).

The second most energetically favorable diffusion path corresponds to the [1 0 0] (or [0 1 0]) direction. In this case, the energy barrier for He moving between two energy minima perpendicular to the *c*-axis ($\Delta E^*_{[100]}$) is ~3.5 times higher than along the [0 0 1], 44.8 kJ mol^{-1}, and ~18 $k_B T$, at room temperature. This higher activation energy barrier is expected, as no continuous channels for He diffusion occur along this direction in zircon (Fig. 3d). In the absence of a continuous path along [1 0 0], the mechanism of diffusion

along this direction involves two steps. First, a He atom residing in a [0 0 1] channel must pass first through the cavities that are left between the chains of alternating [SiO_4] tetrahedra and [ZrO_8] triangular dodecahedra (see the offset of these chains in Fig. 3d, blocking the free movement of He along [1 0 0]). Then the He atom has to move along the [0 0 1] direction until it finds another cavity to pass to the next [0 0 1] channel, and so on. In both the [0 0 1] and [1 0 0] directions, the diffusion of He atoms of ~1 Å diameter is facilitated by the relatively large size of the open cavities (2.4×2.4 Å^2 cross-section for [0 0 1] direction, and $\sim 3.7 \times 3.0$ Å^2 for the [1 0 0] direction, Fig. 3a and d, respectively).

In contrast, diffusion along [1 0 1] is not favored ($\Delta E^*_{[101]} = 101.7$ kJ mol^{-1}), although the geometry of the structure reveals open channels for diffusion ($\sim 2 \times 2$ Å^2 wide, Fig. 3b). This apparent inconsistency can be explained in terms of the most energetically favorable path for He diffusion. At a certain temperature, the He atom will move along the direction in which the energy barrier is lowest. Therefore, instead of moving diagonally along the [1 0 1] channels, He will move along the two most favorable orientations, i.e. [0 0 1] and/or [1 0 0]. This is consistent with the fact that the [1 0 1] open cavities are smaller than the [0 0 1] and [1 0 0] cavities, limiting the movement of He atoms along this path. Finally, movement of He along the [1 1 0] direction is not favored ($\Delta E^*_{(110)} = 421.3$ kJ mol^{-1}), as the open channels for diffusion are narrower ($\sim 1.5 \times 0.3$ Å^2) than the diameter of a He atom (Fig. 3c).

Molecular dynamics simulations are in close agreement with the previous static energy barrier results, as shown in Fig. 5 (and Movies 1–5). A pronounced anisotropy for He diffusion in zircon is observed at low temperatures (<650 K), as He diffusion along the [0 0 1] direction dominates the other diffusion pathways. The motion of interstitial He along the open channels parallel to the *c*-axis is favored by the low energy barrier calculated for that particular crystallographic direction. In contrast, the movement of He perpendicular to the *c*-axis is energetically hindered at low temperatures (Movie 1). Our MD data show that diffusion along the plane perpendicular to the *c*-axis (e.g., along [1 0 0]) is thermally activated, and He hopping from one channel to the adjacent one occurs only above a limiting temperature of 450 K (~180 °C) in perfectly crystalline zircon (Movie 2). As the temperature is increased, the rate at which He hops along the [1 0 0] direction increases as well (Movie 3). At the highest temperatures applied in the MD simulation experiments (850 and 1050 K), He diffuses throughout the zircon structure with no preference for either the [0 0 1] or [1 0 0] crystallographic directions (Movies 4 and 5). No diffusion of He is predicted along the diagonal [1 0 1] and [1 1 0] directions, at any temperature.

4.2. Estimation of He diffusivities

In order to quantify the diffusion rates of He in zircon as a function of temperature and structure, we have estimated the He *tracer diffusion coefficients*, D_{tracer}, (or tracer diffusivities) along specific crystallographic directions by using the energy barrier results presented in Table 3. The term "tracer diffusion" (also called self-diffusion by some authors) is restricted to the particular simple situation in which a tracer isotope (in this case a single ^{4}He atom) in very dilute concentration diffuses interstitially in a homogeneous crystal (in this case, diffusion of a single He atom in a $3 \times 3 \times 3$ supercell of a perfectly crystalline zircon lattice) with no driving forces other than the thermal motion of the tracer itself (Lasaga, 1998).

For a one-dimensional case, the vibrational or hopping attempt frequency v of a He atom between interstitial sites in the zircon structure, in its equilibrium position (before diffusion) is (Glicksman, 2000):

$$v = \frac{1}{\sqrt{2}} \left(\frac{\Delta E^*}{m\lambda^2} \right)^{1/2} \tag{2}$$

where m is the atomic weight of He, ΔE^* is the energy barrier, and λ is the jump distance of the He atom (i.e., the width of the [0 0 1], [1 0 0], [1 0 1], or [1 1 0] energy bumps in Fig. 4, depending on the orientation). The frequency at which the diffusing He atom succeeds in moving from one equilibrium site to an adjacent one is much less than its vibrational frequency at its equilibrium site. Therefore, the "jump frequency" w is calculated by considering that the Boltzmann factor $\exp(-\Delta E^*/k_B T)$ represents the fraction of the vibrations of the diffusing He atom that succeed in surmounting the energy barrier ΔE^*. The jump frequency along a certain crystallographic orientation can then calculated at different temperatures by

$$w = v \exp\left(-\frac{\Delta E^*}{k_B T} \right) \tag{3}$$

By knowing w, the tracer diffusion coefficient of He in zircon can be calculated using Einstein's equation (Glicksman, 2000), which is derived next.

Along a certain crystallographic direction (e.g., along [0 0 1], labeled "*c*"), the linear density of He atoms $n(c)$ is related to the concentration C_{He} (atoms per unit length) by the equation $C_{\text{He}} = n(c)/\lambda_{[001]}$. The flux rates ($J$) at which He atoms jump from above and below their equilibrium positions along [0 0 1] are, respectively:

$$J^+_{\text{He}} = n(c) w_{[001]} \tag{4}$$

$$J^-_{\text{He}} = n(c + \lambda_{[001]}) w_{[001]} \tag{5}$$

The net flux J_{He} is:

$$\begin{aligned} J_{\text{He}} &= J^+_{\text{He}} - J^-_{\text{He}} = (n(c) - n(c + \lambda_{[001]})) w_{[001]} \\ &= \lambda_{[001]} (C_{\text{He}}(c) - C_{\text{He}}(c + \lambda_{[001]})) w_{[001]} \end{aligned} \tag{6}$$

Expanding the term $C_{\text{He}}(c + \lambda)$ in a one-term Taylor series about c coordinate,

$$C_{\text{He}}(c + \lambda_{[001]}) = C_{\text{He}}(c) + \left(\frac{\partial C_{\text{He}}}{\partial c} \right) \lambda_{[001]} \tag{7}$$

gives the net flux of He along the *c*-axis to (Glicksman, 2000):

$$J_{\text{He}} = -\left(\lambda^2_{[001]} w_{[001]} \right) \left(\frac{\partial C_{\text{He}}}{\partial c} \right) \tag{8}$$

By comparing Eq. (8) with Fick's first law $J = -D(\partial C/\partial c)$, the microscopic tracer diffusion coefficient of He along the [0 0 1] direction is defined by the Einstein equation (Lasaga, 1998; Glicksman, 2000):

$$D^{[001]}_{\text{tracer}} = \lambda^2_{[001]} w_{[001]} \tag{9}$$

The quantity $w_{[001]}$ is a one-way jump frequency; therefore, the "total jump frequency" (i.e., diffusing atom jumps to any available adjacent site along the *c*-axis) becomes (Van den Broeke and Krishna, 1995):

$$D^{[001]}_{\text{tracer}} = \frac{1}{2}\lambda^2_{[001]} w_{[001]} \tag{10}$$

4.3. Calculated Arrhenius plots and comparison to laboratory experiments

The tracer diffusion coefficients (D_{tracer}) for He along different crystallographic orientations in perfectly crystalline zircon (i.e., no defects and/or radiation damage), calculated using Eq. (10) are:

$$D^{[001]}_{\text{tracer}} = 0.003\ [\text{cm}^2\ \text{s}^{-1}] \exp\left(-\frac{13.4\ [\text{kJ mol}^{-1}]}{RT}\right) \tag{11}$$

$$D^{[100]}_{\text{tracer}} = 0.003\ [\text{cm}^2\ \text{s}^{-1}] \exp\left(-\frac{44.8\ [\text{kJ mol}^{-1}]}{RT}\right) \tag{12}$$

$$D^{[101]}_{\text{tracer}} = 0.06\ [\text{cm}^2\ \text{s}^{-1}] \exp\left(-\frac{101.7\ [\text{kJ mol}^{-1}]}{RT}\right) \tag{13}$$

$$D^{[110]}_{\text{tracer}} = 0.02\ [\text{cm}^2\ \text{s}^{-1}] \exp\left(-\frac{421.3\ [\text{kJ mol}^{-1}]}{RT}\right) \tag{14}$$

The Arrhenius relations above are plotted in Fig. 6. At room temperature, the diffusivity of He along the most energetically favorable direction [0 0 1] (energy barrier of 13.4 kJ mol^{-1}) is orders of magnitude higher than the other calculated diffusivities ([1 0 0], [1 0 1], and [1 1 0]). This is in close agreement with MD simulations showing the diffusion of He along the *c*-axis below 450 K (~180 °C) (Fig. 5a–c, Movie 1). At 300 K, the difference between $D^{[001]}_{\text{tracer}}$ and $D^{[100]}_{\text{tracer}}$ is five orders of magnitude, as seen on the inset in Fig. 6. As the temperature increases, the difference between the He diffusivities along [0 0 1] and [1 0 0], the most favorable pathways for diffusion of He in the zircon structure, becomes significantly smaller (Fig. 6, inset). At 1050 K (~780 °C), the diffusivities parallel and perpendicular to the *c*-axis ($D^{[001]}_{\text{tracer}}(1050\ \text{K}) = 6.14 \times 10^{-4}\ \text{cm}^2\ \text{s}^{-1}$ and $D^{[100]}_{\text{tracer}}(1050\ \text{K}) = 1.73 \times 10^{-5}\ \text{cm}^2\ \text{s}^{-1}$, respectively) differ by only one order of magnitude (Fig. 6, inset).

It is important to note, that the calculated tracer diffusivities (D_{tracer}) reported in this study account for the diffusion of a single He atom as a tracer component in perfectly crystalline zircon. The tracer diffusivity of a certain isotope is typically measured experimentally using microscopic experimental methods, e.g., nuclear magnetic resonance (NMR) and/or radiotracer techniques (Basser et al., 1994; Kilo et al., 2003). Unfortunately, no experimental measurements of microscopic ^{4}He tracer diffusivities in zircon crystals are available in the literature to compare with our simulation results.

Thus, our calculated tracer diffusivities (D_{tracer}) show significant differences to experimental bulk diffusion data (D_{bulk}) by Reiners et al. (2004). At 1050 K, our calculated

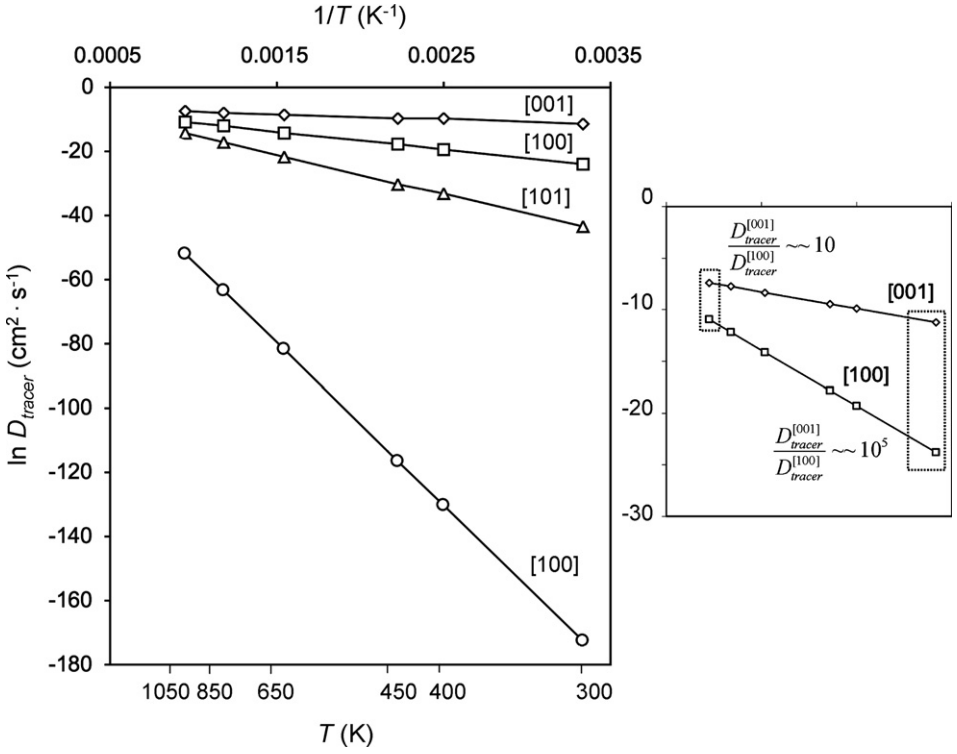

Fig. 6. Arrhenius plot of tracer diffusivities of He in zircon along preferred orientations, as calculated from atomistic results. The inset on the right shows a detail for [0 0 1] and [1 0 0] tracer diffusivities.

tracer diffusivity, e.g., along the most favorable direction ($D^{[001]}_{tracer}(1050\ K) = 6.14 \times 10^{-4}\ cm^2\ s^{-1}$) is ~5 orders of magnitude faster than the bulk experimental diffusivity calculated using Reiners et al. (2004) average activation energy and pre-exponential factors (D_{bulk} $(1050\ K) = 2.74 \times 10^{-9}\ cm^2\ s^{-1}$). These results are consistent with previous studies that report significant differences between tracer and bulk diffusivities, such as Kilo et al. (2003). The cited study shows experimental data on Ca, Y, and Zr isotopes on calcia-stabilized zirconia. They document that ^{88}Y tracer (or self-) diffusivity is five to six orders of magnitude faster than the bulk diffusivity, and its activation energy is also smaller than that of the bulk diffusion. Differences between observed tracer and bulk diffusivities are related to the faster nature of tracer diffusion (e.g., single He atom diffusing in a perfectly crystalline, defect- and radiation damage-free zircon superlattice) relative to bulk/transport diffusion (e.g., collective motion of He atoms under a concentration gradient in macroscopic natural zircon crystals). Unlike the tracer diffusivity, the bulk diffusivity of He in zircon (and other minerals such as apatite and titanite) is measured experimentally using step-heating techniques in which He is sequentially degassed from the crystals, and the ^4He released from the sample in each step is measured by mass spectrometry (Wolf et al., 1996; Farley et al., 1999; Reiners and Farley, 1999; Farley, 2000; Reiners et al., 2004). Such macroscopic laboratory experiments measure the *transport* diffusion of He (hence called "bulk" diffusion), a process that occurs under *non-equilibrium* conditions in the presence of a macroscopic concentration or chemical potential gradient. The diffusion coefficient that accounts for this collective motion of atoms under a concentration gradient is called the transport or bulk diffusion coefficient (D_{bulk}), as opposed to the tracer diffusion coefficient (D_{tracer}), that accounts for the tracer diffusion of a single He atom as a tracer component in zircon under *equilibrium* conditions (Hoogenboom et al., 2000). Therefore, care should be taken when comparing our tracer diffusion rates with bulk diffusion rates, and/or calculating equilibration/residence time of He in zircon within geologic time frames.

Although our atomistic results are not intended to predict diffusion rates at a bulk scale, they throw new light on the mechanisms of diffusion and the differences in diffusion rates along different crystallographic directions (e.g., [0 0 1] faster than [1 0 0]). For example, the anisotropic nature of diffusion that we predict at low temperature can provide an alternative explanation to the non-Arrhenius behavior observed by Reiners et al. (2002, 2004) in the first stages of their He degassing experiments (predictions based on degassing of multiple diffusion domains have been previously invoked by the cited authors to explain this behavior). As it is seen in Fig. 1, a significant inflection in the Arrhenius slope can be observed between ~625 and 670 K (350–400 °C). This kink in the experimental diffusivity may reflect a change in the diffusion mechanisms, as it is deduced from our simulation data. Below ~650 K, our results show that He diffuses anisotropically along the open "channels" parallel to the *c*-axis ([0 0 1]), with a few thermally-activated hop attempts between channels, perpendicular to the *c*-axis, [1 0 0]. Above this limiting temperature, the hop rate for diffusion along [1 0 0] increases leading to a change in the mechanism of diffusion, as He diffuses more isotropically in both the [0 0 1] and [1 0 0]/[0 1 0] directions. Although the crystallographically-controlled nature of He diffusion in zircon can be a reasonable explanation for the observed non-Arrhenius behavior in laboratory experiments, the effects of radiation damage domains (which may be either isolated or interconnected, depending on the degree of damage) and structural imperfections (vacancies, defects) on the atomistic nature of He diffusion in zircon have yet to be investigated in detail.

Unlike the small anisotropy of diffusivity documented for other elements in zircon (e.g., Pb, O, rare eath elements; Cherniak and Watson (2003) and references therein), we predict the diffusion of He in perfectly crystalline zircon to be strongly anisotropic at low temperatures (<450 K). In contrast, diffusion of He becomes close-to isotropic at higher temperatures (>650 K). At these high temperatures, the thermal vibration of the zircon atoms in the simulated zircon structure (see Movies 3–5) leads to a narrowing of the [0 0 1] channels or "pipes", making the flow of He more difficult along this direction and increasing, at the same time, the probability of He atoms hopping between "pipes", along [1 0 0] or [0 1 0].

4.4. Implications of anisotropic diffusion for ZHe thermochronometry

The anisotropic and temperature-dependent behavior of He in zircon presented in this study may have bearing on geologic studies that apply ZHe thermochronometry. Our calculations predict that below ~380 °C (650 K), and hence in a temperature range that includes the closure temperature of He in zircon determined for the ZHe method (~180 °C, Reiners et al., 2004), diffusion of He is predominantly anisotropic. Thus, the influence of the anisotropic nature of He diffusion in thermochronological models has to be evaluated not only for this system, but also for other minerals with anisotropic structural properties such as apatite, titanite, and monazite.

The calculated tracer diffusivities presented in Fig. 6 result in different values of the activation energy (ΔE^* or E_a) and initial diffusity (D_0) along different crystallographic axes. These results are potentially important for geologic applications of ZHe thermochronometry that rely on assumptions of the effective closure temperature for this system. For example, if He diffusion is anisotropic, appropriate values for E_a and D_0 have to be used for calculating cooling-rate dependent effective closure temperatures and/or the temperatures for the top and bottom of the ZHe partial retention zone (e.g., Dodson, 1973; Reiners and Brandon, 2006).

The effect of anisotropy on the effective closure temperature T_c for the ZHe thermochronometer cannot be evaluated using the standard form of the Dodson's formula, because it does not account for multiple values of E_a and D_0 (Dodson, 1973). In addition, our absolute activation energy values in Table 3 cannot be used to quantify T_c because they relate to atomistic tracer diffusion, and hence they do not provide a realistic estimate for comparison to

Table 4
Potential effect of anisotropy (31 kJ mol^{-1} or ~30% difference, this study) on the calculation of an effective closure temperature T_c for ZHe thermochronometer

	E_a (kJ mol^{-1})	E_a (corr) (kJ mol^{-1})	D_0 (cm^2 s^{-1})	Effective T_c* (°C)
Reiners et al. (2004), isotropic	169	169	0.46	188
Incoporating	169 (+30%)	220	0.46	323
±30% due to anisotropy	169 (−30%)	118	0.46	52
Incorporating	169 (+31)	200	0.46	272
±31 kJ mol^{-1} due to anisotropy	169 (−31)	138	0.46	104

Activation energy (E_a) and pre-exponential factor (D_0) taken from Reiners et al. (2004).
* $T_c = E_a/(R\ln[(AR T_c^2 D_0/r^2)/E_a(dT/dt)])$, assuming $(dT/dt) = 10$ °C/Ma, $A = 55$, and $r = 60$ μm.

T_c derived from bulk diffusion experiments (e.g., Reiners et al., 2004). However, here we provide an approximation for how different activation energies obtained from this study can be used to evaluate the potential effect of anisotropy on the bulk experimental E_a and D_0. We report an activation energy difference of ~31 kJ mol^{-1} (~30% difference) between the two more energetically favorable directions for He diffusion, [001] and [100] (Table 3). Results in Table 4 show the potential effect of these variations in E_a on the calculation of an effective closure temperature T_c for a system with isotropic diffusion. This approach, although admittedly a simplified correction procedure, highlights the possible sensitivity of the ZHe system T_c to variations in E_a. Assuming that the effect of anisotropy on the average experimental bulk value of E_a (169 kJ mol^{-1}, Reiners et al., 2004) is ±31 kJ mol^{-1} (or 30% difference), the lower limit of T_c for diffusion along [001] can be estimated to be as low as 52–104 °C, and thus being below the accepted T_c of ~190 °C. This indicates that the product of the form factor and isotropic diffusion constant in the Dodson formula may have to be replaced by a more complex expression that considers the anisotropy. Uncertainties in E_a, D_0, and T_c, zone would then propagate into uncertainties of the exhumation rate and magnitude of exhumation. Thus, more detailed interpretations of the rates of and magnitude of exhumation may be limited by variations in kinetic parameters from anisotropic diffusion (e.g., Ehlers, 2005).

An additional consideration is that the magnitude of anisotropic He diffusion in zircon will likely be acutely sensitive to the extent of radiation damage in the mineral, which modifies the continuity of diffusion pathways along the *c*-axis. This implies that rigorous application of this thermochronometer to bedrock or detrital studies requires that future work will have to determine the sensitivity of kinetic parameters to the degree of radiation damage (Ewing et al., 2003). Some studies have started to address this (Nasdala et al., 2004; Shuster et al., 2006), but further laboratory and computational experiments are needed to measure the diffusivity of He along different crystallographic axes in radiation-damaged zircon.

5. CONCLUSIONS

We applied atomistic empirical force fields, quantum-mechanical and molecular dynamics simulation methods to quantify the diffusion characteristics of He in zircon as a function of crystallographic direction.

1. Energy barriers for He diffusion vary as a function of crystallographic direction in zircon. Diffusion parallel to the *c*-axis ([001] direction) is the most energetically favorable direction ($\Delta E^*_{[001]} = 3.4$ kJ mol^{-1}), follow by the [100] direction (perpendicular to *c*-axis, $\Delta E^*_{[100]} = 44.8$ kJ mol^{-1}).
2. Diffusion of He in zircon is strongly anisotropic at temperatures below 650 K (~380 °C), as He diffuses preferentially along [001]. In contrast, diffusion becomes nearly isotropic above this temperature, as He diffuses in both [001] and [100]/[010] directions.
3. The mechanism of diffusion of He in zircon is temperature-dependent. Below 380 °C (and hence below the effective closure temperature, ~180 °C), He diffuses along the open channels or "pipes" parallel to the *c*-axis, with a few thermally-activated "hop" attempts between channels, along the [100] direction. Above 380 °C, this latter mechanism of diffusion becomes significant and comparable to the former mechanism, as He atoms "hop" between the [001] channels more frequently.
4. Below the closure temperature of He in zircon, diffusion is strongly anisotropic as the calculated tracer diffusivities along the two most favorable directions differ by approximately five orders of magnitude ($D^{[001]}_{tracer}/D^{[100]}_{tracer} \sim 10^5$, at $T = 25$ °C). At higher temperatures, He diffusion in zircon becomes nearly isotropic ($D^{[001]}_{tracer}/D^{[100]}_{tracer} \sim 10$, at $T = 580$ °C).
5. The temperature-dependent change in the mechanism of He diffusion in zircon could explain the non-Arrhenius features observed in He degassing laboratory experiments by Reiners et al. (2004), and can potentially impact the geologic applications of ZHe thermochronometry that rely on assumptions of the effective closure temperature for this system.

ACKNOWLEDGMENTS

Support for this research was received from National Science Foundation Grant EAR-0403732 to U.B. Additional support was provided to M.R. through Fulbright-Mecesup and Rackham Graduate School (at U. of M.) fellowships. We kindly acknowledge the constructive and helpful comments by James Kubicki, David Shuster and two anonymous reviewers.

APPENDIX A. SUPPLEMENTARY DATA

Supplementary data associated with this article can be found, in the online version, at doi:10.1016/j.gca.2007.03.033.

REFERENCES

Accelrys (2005) Forcite and Materials Studio 4.0. Accelrys Inc., San Diego, CA 92121-3752.

Basser P. J., Mattiello J., and Lebihan D. (1994) Estimation of the effective self-diffusion tensor from the NMR spin-echo. *J. Magn. Reson.* **103**, 247–254.

Becke A. D. (1993) Density-functional thermochemistry. III. The role of exact exchange. *J. Chem. Phys.* **98**, 5648–5652.

Cherniak D. J., Hanchar J. M., and Watson E. B. (1997a) Rare-earth diffusion in zircon. *Chem. Geol.* **134**, 289–301.

Cherniak D. J., Hanchar J. M., and Watson B. E. (1997b) Diffusion of tetravalent cations in zircon. *Contrib. Mineral. Petr.* **127**, 383–390.

Cherniak D. J., and Watson E. B. (2001) Pb diffusion in zircon. *Chem. Geol.* **172**, 5–24.

Cherniak D. J., and Watson E. B. (2003) Diffusion in zircon. *Rev. Mineral. Geochem.* **53**, 113–143.

Devanathan R., Corrales L. R., Weber W. J., Chartier A., and Meis C. (2004) Molecular dynamics simulation of disordered zircon. *Phys. Rev. B* **69**, 0641151–0641159.

Dodson M. H. (1973) Closure temperature in cooling geochronological and petrological systems. *Contrib. Mineral. Petr.* **40**, 259–274.

Dove M. T. (2001) Computer simulations of solid solutions. *Eur. Mineral. Union Notes Mineral.* **3**, 225–250.

Ewing R. C., Meldrum A., Wang L. M., Weber W. J., and Corrales L. R. (2003) Radiation effects in zircon. *Rev. Mineral. Geochem.* **53**, 387–425.

Ehlers T. A. (2005) Crustal thermal processes and the interpretation of thermochronometer data. *Rev. Mineral. Geochem.* **58**, 315–350.

Farley K. A. (2000) Helium diffusion from apatite: general behavior as illustrated by Durango fluorapatite. *J. Geophys. Res.-Sol. Ea.* **105**, 2903–2914.

Farley K. A. (2002) (U–Th)/He dating: techniques, calibrations, and applications. *Rev. Mineral. Geochem.* **47**, 819–844.

Farley K. A., Wolf R. A., and Silver L. T. (1996) The effects of long alpha-stopping distances on (U–Th)/He ages. *Geochim. Cosmochim. Acta* **60**, 4223–4229.

Farley K. A., Reiners P. W., and Nenow V. (1999) An apparatus for high-precision helium diffusion measurements in minerals. *Anal. Chem.* **71**, 2059–2061.

Finch R. J., and Hanchar J. M. (2003) Structure and chemistry of zircon and zircon-group minerals, Zircon. *Rev. Mineral. Geochem.* **53**, 1–25.

Frisch M. J., Trucks G. W., Schlegel H. B., Scuseria G. E., Robb M. A., Cheeseman J. R., Montgomery, Jr., J. A., Vreven T., Kudin K. N., Burant J. C., Millam J. M., Iyengar S. S., Tomasi J., Barone V., Mennucci B., Cossi M., Scalmani G., Rega N., Petersson G. A., Nakatsuji H., Hada M., Ehara M., Toyota K., Fukuda R., Hasegawa J., Ishida M., Nakajima T., Honda Y., Kitao O., Nakai H., Klene M., Li X., Knox J. E., Hratchian H. P., Cross J. B., Bakken V., Adamo C., Jaramillo J., Gomperts R., Stratmann R. E., Yazyev O., Austin A. J., Cammi R., Pomelli C., Ochterski J. W., Ayala P. Y., Morokuma K., Voth G. A., Salvador P., Dannenberg J. J., Zakrzewski V. G., Dapprich S., Daniels A. D., Strain M. C., Farkas O., Malick D. K., Rabuck A. D., Raghavachari K., Foresman J. B., Ortiz J. V., Cui Q., Baboul A. G., Clifford S., Cioslowski J., Stefanov B. B., Liu G., Liashenko A., Piskorz P., Komaromi I., Martin R. L., Fox D. J., Keith T., Al-Laham M. A., Peng C. Y., Nanayakkara A., Challacombe M., Gill P. M. W., Johnson B., Chen W., Wong M. W., Gonzalez C., and Pople J. A. (2004). Gaussian 03, Gaussian, Inc., Wallingford, CT.

Gale J. D., and Rohl A. L. (2003) The General Utility Lattice Program (GULP). *Mol. Simulat.* **29**, 291–341.

Garofalini S. H. (2001) Molecular dynamics simulations of silicate glasses and glass surfaces. *Rev. Mineral. Geochem.* **42**, 131–164.

Glicksman M. E. (2000). *Diffusion in Solids: Field Theory, Solid-State Principles, and Applications*. John Wiley & Sons, New York, 498 p.

Hoogenboom J. P., Tepper H. L., Van der Vegt N. F. A., and Briels W. J. (2000) Transport diffusion of argon in $AlPO_4$-5 from equilibrium molecular dynamics simulations. *J. Chem. Phys.* **113**, 6875–6881.

Kilo M., Taylor M. A., Argirusis C. h., Borchardt G., Lesage B., Weber S., Scherrer S., Scherrer H., Schroeder M., and Martin M. (2003) Cation self-diffusion of 44Ca, 88Y, and 96Zr in single-crystalline calcia- and yttria-doped zirconia. *J. Appl. Phys.* **94**, 7547–7552.

Lasaga A. C. (1998) *Kinetic Theory in the Earth Sciences*. Princeton University Press, New Jersey, 811 p.

Maca F., Kotrla M., and Trushin O. S. (1999) Energy barriers for diffusion on stepped Pt(1 1 1) surface. *Vacuum* **54**, 113–117.

Meldrum A., Boatner L. A., Weber W. J., and Ewing R. C. (1998) Radiation damage in zircon and monazite. *Geochim. Cosmochim. Acta* **62**, 2509–2520.

Nasdala L., Reiners P. W., Garver J. I., Kennedy A. K., Stern R. A., Balan E., and Wirth R. (2004) Incomplete retention of radiation damage in zircon from Sri Lanka. *Am. Mineral.* **89**, 219–231.

Ozkan H., Cartz L., and Jamieson J. C. (1974) Elastic-constants of nonmetamict zirconium silicate. *J. Appl. Phys.* **45**, 556–562.

Palenik C. S., Nasdala L., and Ewing R. C. (2003) Radiation damage in zircon. *Am. Mineral.* **88**, 770–781.

Reiners P. W., and Farley K. A. (1999) Helium diffusion and (U–Th)/He thermochronometry of titanite. *Geochim. Cosmochim. Acta* **63**, 3845–3859.

Reiners P. W., Farley K. A., and Hickes H. J. (2002) He diffusion and (U–Th)/He thermochronometry of zircon: initial results from Fish Canyon Tuff and Gold Butte. *Tectonophysics* **349**, 297–308.

Reiners P. W., Spell T. L., Nicolescu S., and Zanetti K. A. (2004) Zircon (U–Th)/He thermochronometry: He diffusion and comparisons with Ar-40/Ar-39 dating. *Geochim. Cosmochim. Acta* **68**, 1857–1887.

Reiners P. W. (2005) Zircon (U/Th)–He thermochronometry. *Rev. Mineral. Geochem.* **58**, 151–179.

Reiners P. W., and Brandon M. T. (2006) Using thermochronology to understand orogenic erosion. *Annu. Rev. Earth Pl. Sc.* **34**, 419–466.

Robinson K., Gibbs G. V., and Ribbe P. H. (1971) Structure of zircon—comparison with garnet. *Am. Mineral.* **56**, 782–790.

Shuster D. L., Flower R. M., and Farley K. A. (2006) The influence of natural radiation damage on helium diffusion kinetics in apatite. *Earth Planet. Sci. Lett.* **249**, 148–161.

Tagami T., Farley K. A., and Stockli D. F. (2003) (U–Th)/He geochronology of single zircon grains of known tertiary eruption age. *Earth Planet. Sci. Lett.* **207**, 57–67.

Valley J. W., Peck W. H., King E. M., and Wilde S. A. (2002) A cool early Earth. *Geology* **30**, 351–354.

Van den Berg A. W. C., Fikkema E., Jansen J. C., and Bromley S. T. (2005) Self-diffusion of molecular hydrogen in cathrasils compared: dodecasil 3C versus sodalite. *J. Chem. Phys.* **122**, 204710–204716.

Van den Broeke L. J. P., and Krishna R. (1995) Experimental verification of the Maxwell-Stefan theory for micropore diffusion. *Chem. Eng. Sci.* **50**, 2507–2522.

Watson E. B., and Cherniak D. J. (1997) Oxygen diffusion in zircon. *Earth Planet. Sci. Lett.* **148**, 527–544.

Watson E. B., and Harrison T. M. (2005) Zircon thermometer reveals minimum melting conditions on earliest Earth. *Science* **308**, 841–844.

Weber W. J., Ewing R. C., and Wang L. M. (1994) The radiation-induced crystalline-to-amorphous transition in zircon. *J. Mater. Res.* **9**, 688–698.

Wolf R. A., Farley K. A., and Silver L. T. (1996) Helium diffusion and low-temperature thermochronometry of apatite. *Geochim. Cosmochim. Acta* **60**, 4231–4240.